Journal of Alloys and Compounds 576 (2013) 302–316

Contents lists available at SciVerse ScienceDirect

Journal of Alloys and Compounds

journal homepage: www.elsevier.com/locate/jalcom

Ab initio study of the cohesive properties, electronic structure and thermodynamic stability of the Ni–In and Ni–Sn intermetallics

S. Ramos de Debiaggi [a,b,*], C. Deluque Toro [a], G.F. Cabeza [b,c], A. Fernández Guillermet [b,d]

[a] *Facultad de Ingeniería, Universidad Nacional del Comahue, Buenos Aires 1400, 8300 Neuquén, Argentina*
[b] *CONICET, Argentina*
[c] *Dpto. de Física, Universidad Nacional del Sur, Alem 1253, 8000 Bahía Blanca, Argentina*
[d] *Centro Atómico Bariloche e Instituto Balseiro, Avda. Bustillo 9500, 8400 Bariloche, Argentina*

ARTICLE INFO

Article history:
Received 30 December 2012
Received in revised form 26 February 2013
Accepted 2 March 2013
Available online 10 April 2013

Keywords:
Ab initio calculations
Ni–In and Ni–Sn alloys
Thermodynamic properties
Lead-free soldering alloys

ABSTRACT

A comprehensive study of the structural, cohesive and electronic properties of several stable, metastable and non-stable intermetallic phases (IPs) of the Ni–In and Ni–Sn systems have been performed by *ab initio* density-funcional-theory (DFT) methods. Using the projector augmented wave method we have performed systematic spin polarized calculations with the exchange and correlation functions of Perdew and Wang in the generalized gradient approximation (GGA), as well as those by Ceperley and Alder in the local-density-approximation (LDA). Structural properties, the energy-of-formation (EOF) from the elements and the cohesive properties of the various phases have been established by minimizing the internal structural parameters. We present trends at 0 K in the composition dependence of the molar volumen, bulk modulus and its pressure derivative, electronic density of states, magnetic moments and the EOF of several stable and metastable IPs reported in the Ni–In and Ni–Sn systems as well as various non-stable (hypothetical) compounds which are relevant in connection with the thermodynamic analysis of the Ni–In and Ni–Sn systems using Gibbs energy models and the so-called CALPHAD techniques. The results are compared with the available experimental data and with previously reported theoretical results. The present study of the thermodynamic and cohesive properties of Ni–In/Sn intermetallic phases should contribute to the understanding of the phase-stability systematics in the Ni–In–Sn system and the design of new soldering alloys.

1. Introduction

The environmental demand for Pb-free soldering systems has motivated a systematic search for candidates to replace the Pb–Sn alloys. In particular, considerable research efforts have been devoted to the study of alloys based on the In–Sn system. More specifically, the In–48 at.%Sn eutectic alloy has been considered attractive because it presents a low liquidus temperature, good wettability and might form various intermetallic phases (IPs) at the interconnection zone [1]. The properties of these IPs, which are formed between the solder alloy and the usual contact materials, determine the final properties of the joints. Although Cu is the most commonly used contact material in electronic devices, Ni is also used as a substrate, since in comparison with Cu it presents a slower kinetics of interfacial reaction with the solder. This prevents the excessive intermetallic growth which is known to have undesirable effects on the mechanical reliability of the joints [2]. Because of this interesting combination of properties, various studies have been devoted to the properties of the IPs occurring in the Ni–In–Sn system [3,4]. However, in spite of the long-standing practical interest in these compounds, there is a need for additional information, to be used with two main theoretical and practical purposes. In the first place, the experimental data available does not allow a comparative study of the properties of the stable IPs and to establish trends in the composition and structure dependence of the molar volume and other equation-of-state (EOS) parameters. These quantities are also of interest, *i.a.*, as variables in various types of correlations involving other elastic and vibrational properties. Secondly, there is a need for information on the phase diagram and thermodynamic quantities used to describe the relative stability of the IPs. The phase-stability problem in multicomponent systems has often been treated by applying the CALPHAD [5] modeling and extrapolation techniques. When applying such methods, the boundaries of the phase-stability fields in, *e.g.*, a ternary system, might be calculated using descriptions of the Gibbs energy function (G) which are based on a suitable combination of the G contributions of the binary subsystems. In many cases, the binary G functions are determined by fitting the

* Corresponding author at: Dpto. de Física, Facultad de Ingeniería, Universidad Nacional del Comahue, Buenos Aires 1400, 8300 Neuquén, Argentina. Tel.: +54 299 4490331; fax: +54 299 4490329.
E-mail addresses: sbramos@yahoo.com, susana.ramos@fain.uncoma.edu.ar (S. Ramos de Debiaggi).

0925-8388/$ - see front matter © 2013 Elsevier B.V. All rights reserved.
http://dx.doi.org/10.1016/j.jallcom.2013.03.047

parameters in the models to the experimental data available. However, the modeling of ternary compounds in the Ni–In–Sn system using, in particular, the Compound-Energy Formalism (CEF) [6] would involve information concerning binary Ni–In and Ni–Sn compounds which are not stable. Therefore, a useful thermodynamic database for the Ni–In–Sn system should also include reliable information on the structural and EOS parameters, as well as the relative stability of the non-stable phases which are hypothesized in standard CALPHAD models such as the CEF. The general purpose of the present work is to rely upon *ab initio* methods to develop such a database for the Ni–In and Ni–Sn subsystems of the ternary. The new theoretical information will be used to study trends in the cohesive, electronic and phase-stability properties of various stable and metastable stoichiometric IPs, as well as the hypothetical compounds involved in the thermodynamic modeling of the key non-stoichiometric Ni–In and Ni–Sn phases. To this end, extensive density-functional-theory (DFT) calculations have been performed of the 0 K lattice-parameters, molar volume, bulk modulus and its pressure derivative, electronic density of states, magnetic moments and the energy of formation from the elements of several stable and non-stable Ni–In and Ni–Sn compounds. In the remainder of the present section we review the experimental and theoretical information on the Ni–In and Ni–Sn systems and explain the specific motivations and aims of the work.

The phase diagram of the Ni–In system [7] presents eight stable solid phases: Ni_3In (hexagonal hP8), Ni_2In (hexagonal hP6), $Ni_{13}In_9$ (monoclinic mC44), NiIn (hexagonal hP6 with CoSn prototype structure) and Ni_2In_3 (hexagonal hP5), and $Ni_{28}In_{72}$ (cubic cI52 or cI40) are stable at low temperature, whereas ξ-Ni_2In (hexagonal hP4) and δ-NiIn (cubic cP2) non-stoichiometric phases are stable only at high temperatures. In thin films and at high pressures the cubic cP4 $AuCu_3$ prototype structure has been observed [8]. In a later revision of the Ni–In phase diagram [9] based on X-ray diffraction (XRD) data only the Ni_3In hP8 structure could be confirmed. For the other phases, like the low temperature NiIn and Ni_2In_3 ones, the calculated XRD spectra do not precisely fit the observed X-rays data. For the composition range around Ni_2In recent experimental investigations indicate that the ideal, fully occupied Ni_2In-hP6 structure, does not exist as a stable room-temperature phase but completely dissociates into the previosuly unreported Ni_7In_3 and Ni_5In_3 stoichiometric compounds [10]. The compound Ni_7In_3 (triclinic aP40) is isostructural with Cu_7In_3, a B8 superstructure phase with ordered In vacancies. The phase with composition Ni_5In_3 (monoclinic mC32) is isostructural with Ni_5Ge_3, which in turn is a Ni deficient B8 superstructure relative to Ni_2In. In a later work it was reported that the compound Ni_5In_3 is not stable at the annealing temperature of 400 °C, which is 80 °C below the reported transition temperature from Ni_5In_3 to the high temperature $Ni_{2\pm x}In$ phase [11]. Instead it forms a two-phase mixture of Ni_7In_3 and $Ni_{13}In_9$. Although it is possible that the Ni_5In_3 phase exists in the Ni–In system, it might be a metastable compound or a phase stable at temperatures different from the one studied in Ref. [11]. In spite of these new findings no changes in the phase relationships were introduced by these authors to the phase diagram previously established by Singleton and Nash [7] and Durussel et al. [9].

Ab initio methods have previously been applied to some selected phases of the Ni–In system. The electronic structure, mechanical and magnetic properties of Ni_3In has been studied by Guo et al. [12,13] using the full-potential linear augmented plane wave (FP-LAPW) [14] method and the generalized gradient approximation (GGA) potentials of Purdew, Burke and Ernzerhof (PBE) [15]. The ferromagnetic cP4 phase is reported to be the ground state with respect to the hP8, the known stable phase at low temperature, and the tetragonal tI8 phase [13]. The calculated lattice parameters are in good agreement with experiments, and both cP4 and hP8 phases are predicted to be weak ferromagnets with magnetic moments of 0.5 and 0.7 μ_B/cell, respectively. Hsu et al. [16] measured the X-ray absorption near-edge spectroscopy (XANES) spectra at the Ni K-, In L_3-, and In K-edge of Ni_3In and $Ni_{13}In_9$, and compared with theoretical XANES spectra and site- and momentum-decomposed partial DOS derived from first-principles FP-LAPW calculations. The theoretical XANES spectra of Ni_3In calculated for the hP8 structure resembles the corresponding experimental spectra much better than those calculated for the cP4 and tI8 structures. However, the calculated spectra for the $Ni_{13}In_9$ phase, modeled as an orthorhombic structure with 22 atoms in the unit-cell instead of the monoclinic mC44 structure reported for this compound [8] agreed poorly with the experimental data. Also to note is that in these previous works no relaxation of the internal coordinates in the unit cell was allowed for. In a very recent work using the same spin polarized FP-LAPW method and GGA approximation, and taking into account the full relaxation of internal coordinates, Deluque Toro et al. [17] established that the hexagonal Ni_3In (hP8), Ni_2In (hP6), NiIn (hP6) and Ni_2In_3 (hP5) phases are thermodynamically stable with respect to the elements, and that the NiIn (hP6) phase is the one with the lowest energy. Only for the Ni_3In compound a permanent magnetic moment, with a calculated value of 1.13 μ_B/cell, was determined. The NiIn CoSn-type intermetallic has been studied both experimentally and by first-principles calculations by Mikhaylushkin et al. [18]. They used the projector augmented wave method [19] and the GGA [20]. The structural parameters for the ground state structure agree well with the experimental data. NiIn is reported to be paramagnetic. High-temperature multianvil experiments indicate that NiIn transforms into a CsCl-type high-pressure phase, in accord with the theoretical prediction.

In the present *ab initio* study we will treat the low-temperature stable phases Ni_3In, Ni_2In, $Ni_{13}In_9$, NiIn, Ni_2In_3 and Ni_3In_7. Moreover, we will study the new compounds Ni_7In_3 and Ni_5In_3, which are not included in the phase diagram but have been detected around the Ni_2In composition range [10]. In addition to these stable and metastable stoichiometric phases, the non-stable (“hypothetical”) compounds involved in the CALPHAD modeling of the $Ni_{13}In_9$, ξ-Ni_2In and δ-NiIn non-stoichiometric phases using sublattice models (see below) will be treated. With this new information a comprehensive *ab initio* account of the Ni–In system, involving stable, metastable and hypothetical, model-generated compounds, will be presented for the first time. In addition, the Ni–In results will be compared with the corresponding properties of the closely related Ni–Sn system, which is reviewed in the following.

Three intermetallic phases are included in the accepted Ni–Sn phase diagram [21]: Ni_3Sn, Ni_3Sn_2, and Ni_3Sn_4. The Ni_3Sn compound occurs in two forms, *viz.*, the high temperature (HT) cubic cF16 and the low temperature (LT) hexagonal hP8 forms. Two other structures of Ni_3Sn have also been reported: the cubic cP4 type, stable at high pressures, and the orthorhombic oP8 type, which forms by a martensitic transformation of the Ni_3Sn (HT) phase [22]. There are also two forms of Ni_3Sn_2 in the phase diagram, *viz.*, the Ni_3Sn_2 (HT), a Ni_2In/NiAs $B8_2/B8_1$ type structure, stable between 873 and 1540 K, and the Ni_3Sn_2 (LT) structure stable below 873 K [21]. Three forms of Ni_3Sn_2 (LT) have been identified, one commensurate and two incommensurate ones [23–27]. The commensurate phase, stable between 39.3 and 40.8 at.%Sn, has an orthorhombic oP20 structure and lies between the two incommensurate phases, Ni_3Sn_2 (LT′) with orthorhombic symmetry and Ni_3Sn_2 (LT″) with unknown crystallographic characteristics. Only the commensurate phase will be studied in this work. The Ni_3Sn_4 compound has a monoclinic mC16 symmetry, isostructural with CoGe, but with partial occupation of Ni 2c sites to fit with the compound stoichiometry [28]. Previous works reported a monoclinic structure with fully occupied mC14 symmetry [8]. Metastable

crystalline phases have also been reported for this system. In studies of interfacial reactions in Ni/Sn using diffusion couples, Boettinger et al. [29] detected the $NiSn_4$ phase in solder joints subjected to thermal cycles. This phase, isomorphous to $AuSn_4$, presents the orthorhombic oC20 symmetry. At the same composition Watanabe et al. [30] identified a tetragonal phase in Ni–Sn thin films obtained by electrodeposition. The cohesive properties of various stable, metastable and hypothetical ("virtual") Ni–Sn intermetallics have been studied by Ghosh using first principles DFT calculations, ultrasoft pseudopotentials (US-PP) and both the LDA and GGA for the exchange–correlation functional [31]. The ground state structures are found to be consistent with experimental observations. The metastable compound $NiSn_4$-oC20, observed in Ni/Sn reaction couples, is predicted to be a ground state structure and its mechanical stability was corroborated by calculating the single-crystal elastic constants. Since a tetragonal phase is also observed in Ni–Sn thin films [30] the $NiSn_4$-tP10 structure was also treated by Ghosh [31]. Its thermodynamic stability is predicted to be similar to that of $NiSn_4$-oC20. For the ground state compounds the energy of formation calculated using US-PP and LDA agree better with calorimetric data than those calculated using US-PP and GGA. The experimental lattice parameters of the stable and metastable phases are found to lie between those calculated using LDA and GGA. In several cases, the values obtained by GGA agree within 1% with the measured ones. A similar trend has recently been observed in *ab initio* calculations performed in the closely related Cu–In and Cu–Sn systems [32].

Some of the compounds treated by Ghosh [31] were included in the present work, for two reasons. A first reason, a general one, is that we aim at establishing and comparing the trends in the calculated properties of the Ni–In and Ni–Sn stable and metastable compounds. Such comparison requires that both systems are treated using the same computational scheme and level of approximation. The second reason, a more specific one, is that the present work is conceived as a first step in the development of a thermodynamic database to be used as a complement of the CALPHAD-type assessment ("optimization") procedures [33]. To this end the properties of the stable and non-stable phases hypothesized in the CALPHAD models for Ni–Sn compounds (see below) should also be calculated using the same computational scheme and level of approximation. For these reasons, the low-temperature stable phases Ni_3Sn, Ni_3Sn_2, Ni_3Sn_4, the metastable $NiSn_4$ phase and the hypothetical phases involved in the most recent CALPHAD analysis of the Ni–Sn system, were included in the present study.

A key purpose of the present work is to produce thermodynamic information of direct interest for the thermodynamic modeling of binary and ternary IPs using the CEF, a rather general

Table 1
Crystallographic data and typical composition of the stable and metastable Ni–In and Ni–Sn phases treated in the present work.

System	Phase (typical composition)	Pearson symbol
Ni–In	Ni_3In (25 at.% In)	cP4
	Ni_3In (25 at.% In)	hP8
	Ni_3In_7 (30 at.% In)	aP40
	Ni_2In (33.33 at.% In)	hP6
	Ni_5In_3 (37.5 at.% In)	mC32
	$Ni_{13}In_9$ (40.9 at.% In)	mC44
	NiIn (50 at.% In)	hP6
	Ni_2In_3 (60 at.% In)	hP5
	Ni_3In_7 (70 at.% In)	cI40
Ni–Sn	Ni_3Sn (25 at.% Sn)	cF16
	Ni_3Sn (25 at.% Sn)	hP8
	Ni_3Sn (25 at.% Sn)	cP4
	Ni_3Sn_2 (40 at.% Sn)	oP20
	Ni_3Sn_4 (57.14 at.% Sn)	mC14
	$NiSn_4$ (80 at.% Sn)	oC20

modeling scheme that involves the identification of the sublattices where the mixing of the alloying elements takes place [6]. In particular, Waldner and Ipser [34] treated the δ-NiIn phase of the Ni–In system using the two-sublattice model $(Ni,Va)_1(In,Ni)_1$ whereas the ζ-Ni_2In and ζ'-$Ni_{13}In_9$ phases were described using the three-sublattice schemes $(Ni)_1(Ni,Va)_1(In,Ni)_1$ and $(Ni)_1(Ni,Va)_1(In)_1$, respectively. In these formulas, the elements in parentheses substitute for each other in the given sublattice and "Va" represents vacant crystalline sites. When applying the CEF [6] with these sublattice schemes it is necessary to determine the thermodynamic properties of the hypothetical "end-member compounds" (EMC) which are generated by assuming that each sublattice is fully occupied by one of the mixing elements (Ni, In and Sn) or by Va. The EMC for the Waldner and Ipser model for ζ'-$Ni_{13}In_9$ correspond to the sublattice occupations $(Ni)_1(Ni)_1(In)_1$, usually represented as "Ni:Ni:In", and interpreted as a compound with formula "Ni_2In"; and to the sublattice occupations $(Ni)_1(Va)_1(In)_1$, *i.e.*, Ni:Va:In, which represent a "NiIn" compound. In current CALPHAD work the energy and entropy parts of the Gibbs energy of formation of the EMC are usually determined by fitting the CEF equations to various types of experimental data. As an alternative, the energy of formation of these hypothetical compounds will be calculated in the present study and critically compared with the values obtained by Waldner and Ipser [34] for the Ni–In system and by Liu et al. [35] for the Ni–Sn system using CALPHAD techniques. On this basis, a discussion will be presented of the possible use of theoretical methods to complement the thermodynamic optimization techniques with *ab initio* information on Ni–In and Ni–Sn IPs, and to

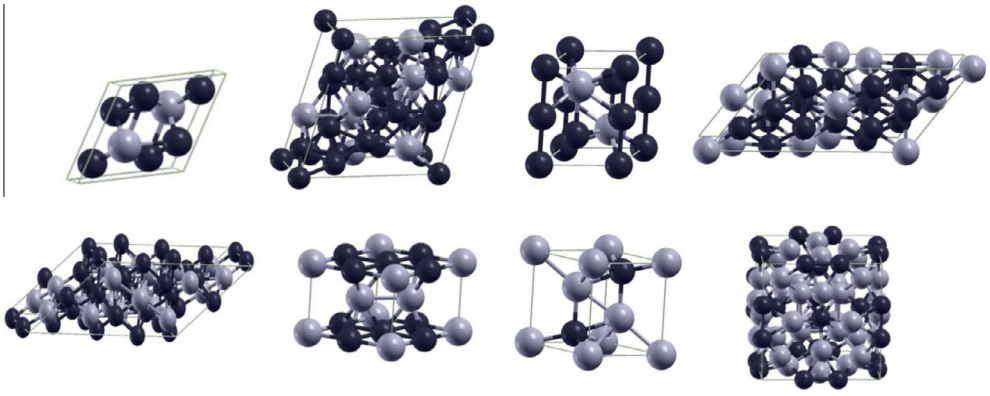

Fig. 1. Structures of the Ni–In intermetallic phases treated in the present work. From left to right: Ni_3In (hP8), Ni_7In_3, Ni_2In, Ni_5In_3, $Ni_{13}In_9$, NiIn, Ni_2In_3, Ni_3In_7. Black and light gray spheres represent Ni and In atoms, respectively.

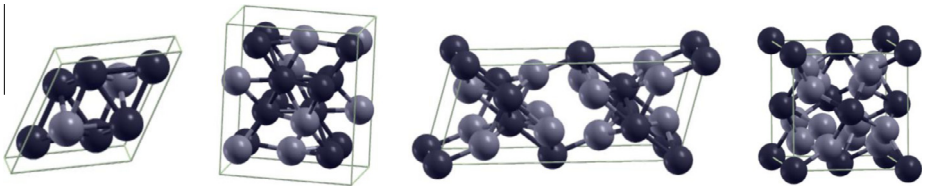

Fig. 2. Structures of the Ni–Sn intermetallic phases treated in the present work. From left to right: Ni_3Sn, Ni_3Sn_2, Ni_3Sn_4, $NiSn_4$. Black and dark spheres represent Ni and Sn atoms, respectively.

gain insight upon the effect of the approximations involved in the estimation procedures adopted in current CALPHAD modeling work.

The crystallographic data corresponding to the stable and metastable Ni–In and Ni–Sn IPs studied in this work are summarized in Table 1. The corresponding structures are shown in Figs. 1 and 2. The hypothetical EMC included in the present work are discussed in Section 3.5.

2. Theoretical method

Spin polarized total energy DFT calculations were performed using the projector augmented-wave method (PAW) [19] and the VASP code [36].

For the exchange–correlation energy we adopted the generalized gradient approximation due to Perdew and Wang (GGA-PW91) [20] and the local density approximation due to Ceperley and Alder [37]. It is expected that these approximations will give different results for the cohesive and structural properties of solids. The LDA, which is valid for systems with slowly varying electronic densities, it is known to overbind the atoms in the solid, predicting lattice-parameters (LPs) that are typically understimated while the cohesive energies and elastic moduli are typically overestimated [38]. The GGA includes a electronic density gradient term in the LDA exchange–correlation energy, greatly improving the accuracy for the cohesive properties of solids, especially for binding energies [39]. However, it very frequently overcorrects LDA results yielding LPs and bulk moduli that are overestimated and underestimated respectively [40]. When comparing predictions of the energy of formation from the elements (EOF), it has been found in previous calculations for systems related to the present ones that switching from GGA to LDA leads to a decrease of (*i.e.*, to a more negative) EOF by a few kJ/mol. As a consequence, the LDA predictions of the EOF are in better agreement with experiments [32,45,46,48]. In the present work we will critically compare the results of the specific LDA and GGA exchange–correlation energy functions adopted to calculate the cohesive and structural properties for the Ni–In and Ni–Sn IPs. For the PAWs we considered 10 valence electrons for Ni ($3d^84s^2$), 3 for In ($5s^2p^1$) and 4 for Sn ($5s^2p^2$). The kinetic energy cut-off for the plane wave expansion of the electronic wavefunction was 330 eV. In order to test the effect of this choice for the cutoff energy upon the total energies and the energy of formation of the compounds, (Section 3.4) calculations were performed using a cut-off energy of 450 eV for the Ni_3In (hP8) compound and the corresponding elements. The changes in the total energy are less than 10 meV/atom (1 kJ/mol), and the energies of formation are converged within 2 meV/atom (0.2 kJ/mol) when adopting a cut-off energy of 330 eV.

We used the Monkhorst–Pack k-point meshes [41] and the Methfessel–Paxton technique [42] with a smearing factor of 0.1 for the electronic levels. The convergence of the k-point meshes was checked until the energy converged with a precision better than 1 meV/atom. In this way the k-meshes considered were $15 \times 15 \times 19$ for Ni_3In and Ni_3Sn, $3 \times 3 \times 5$ for Ni_7In_3, $19 \times 19 \times 15$ for Ni_2In, $7 \times 13 \times 13$ for Ni_5In_3, $5 \times 9 \times 7$ for $Ni_{13}In_9$, $17 \times 17 \times 19$ for NiIn, $17 \times 17 \times 15$ for Ni_2In_3, $7 \times 7 \times 7$ for Ni_3In_7; $11 \times 15 \times 9$ for Ni_3Sn_2, $3 \times 9 \times 7$ for Ni_3Sn_4 and $7 \times 7 \times 3$ for $NiSn_4$. These values implied up to 432 k points in the irreducible Brillouin zone (IBZ), depending on the structure. The criterion for the self-consistent convergence of the total energy was 0.1 meV. The structures were optimized with respect to the lattice-parameters and the internal degrees of freedom compatible with the space group symmetry of the crystal structure, until the forces were less than 30 meV/Å and the energy variations with respect to the structural degrees of freedom were better than 1 meV/atom.

The total energy (E) and external pressure (P) were calculated for values of volume (V) varying slightly around the equilibrium (up to ±5%), relaxing all external and internal coordinates of the system. The bulk modulus and its pressure derivative were obtained by fitting the calculated pressure–volume values to the P *vs.* V EOS due to Vinet et al. [43]. This equation is the one adopted in our previous *ab initio* work on Cu–In compounds [44], in the work by Ghosh and Asta on the Cu–Sn system [45] and by Ghosh on Ni–Sn [31] compounds.

The energy of formation (EOF) of the IPs was calculated as

$$\Delta E^{\phi}(Ni_aM_b) = \frac{1}{a+b}E^{\phi}_{Ni_aM_b} - \left[\frac{a}{a+b}E^{\theta}_{Ni} + \frac{b}{a+b}E^{\psi}_{M}\right] \quad (1)$$

where ΔE^{ϕ} is the EOF per atom of the Ni_aM_b (with M = In, Sn) compound with the structure ϕ, $E^{\phi}_{Ni_aM_b}$ the corresponding total energy, $E^{\theta}_{Ni}$is the total energy per atom of Ni in its equilibrium phase θ (fcc), and E^{ψ}_{M} is the total energy per atom of In or Sn in their equilibrium structure ψ (ψ = tI2 for In and tI4 for Sn, see below). This choice of the reference states allows a direct comparison of the theoretical ΔE^{ϕ} with the results of calorimetric experiments and with the values derived in the CALPHAD modeling of phase diagrams. A negative EOF means that the compound is thermodynamically stable with respect to the elements a 0 K. This is the expected behavior of the IPs which are observed as stable phases at very low temperatures in the phase diagram.

3. Results and discussion

3.1. Cohesive properties of the elements

In Table 2 we summarize the results for the elements Ni, In and Sn in their known equilibrium structures, *i.e.*, fcc for Ni, tI2 for In and tI4 for Sn. We report the LPs, the equilibrium volume (V_o), the bulk modulus (B_o) and its pressure derivative (B'_o).

The LPs are underestimated by less than 2.4% by the LDA, and overestimated by less than 2.2% in GGA calculations. The present LPs agree very well with previous *ab initio* results based on US-PP [31] and FP-LAPW [17] calculations. In general, the calculated

Table 2
Calculated structural, equation-of-state parameters and magnetic moments for pure elements Ni, In and Sn at 0 K. The lattice parameters are given in Å, the equilibrium volume (V_o) in Å^3/atom, the bulk modulus (B_o) in GPa, the magnetic moment in μ_B/atom.

Pure	P.S.	V_o	a, c	B_o	B'_o	M	Aprox.
Ni	cF4	10.044	3.425	257.9	5.6	0.586	LDA
		(10.141	3.436	251.4	4.5	0.594)[a]	
		(10.016	3.422	255.8	5.0	0.56)[b]	
		10.931	3.523	186.2	5.9	0.607	GGA
		(11.026	3.533	197.0	6.7	0.651)[a]	
		(10.940	3.524	201.4	3.6	0.59[b]	
			3.510[c]	187.6[d]	5.3[e]	0.604[f]	
			3.515[g]		4.8[e]	0.615[h]	
In	tI2	24.769	3.178, 4.905	51.3	5.2	0.0	LDA
		(24.513	3.191, 4.813	50.6	5.4)[b]		
		27.505	3.305, 5.036	36.5	6.3		GGA
		(27.417	3.318, 4.979	35.7	5.3)[b]		
		26.020	3.245, 4.942[i]	41.8[j]	4.8[j]		
Sn	tI4	26.193	5.794, 3.121	61.5	5.1	0.0	LDA
		(26.173	5.780, 3.134	59.8	5.0)[a]		
		28.348	5.948, 3.204	48.6	5.9		GGA
		(28.443	5.947, 3.218	46.0	4.3)[a]		
		26.886	5.820, 3.175[i]	57.9[k]	6.01[e]		
					4.96[e]		

[a] *Ab initio* US-PP [31].
[b] *Ab initio* FP-LAPW [17].
[c] Experimental data extrapolated at 0 K [53].
[d] Experimental data based on C_{ij} at 0 K [54].
[e] Reported data at 298 K [55].
[f] Experimental data at 0 K [56].
[g] Experimental data extrapolated to 0 K [57].
[h] Reported data at 0 K [58].
[i] Experimental data [8].
[j] Experimental data at 293 K [59].
[k] Experimental data at 4.2 K [60].

Table 3
Structural and elastic properties for Ni–In intermetallic phases at 0 K. The lattice parameters are given in Å, the equilibrium volume (V_o) in Å^3/atom, the bulk modulus (B_o) in GPa.

Phase Stable	P.S.	V_o	a, b, c, α, β, γ	B_o	B'_o	Aprox.
Ni_3In	hP8	13.188	5.367, 4.229	149.6	6.6	GGA
		(13.128	5.357, 4.227	148.9	4.9)[a]	
		(13.154	5.314, 4.303	156.0)[b]		
		12.130	5.216, 4.119	191.4	6.6)	LDA
		(12.060	5.207, 4.109	192.7	5.4)[a]	
		(13.031	5.332, 4.234)[c]			Exp.
Ni_3In	cP4	13.152	3.747	151.1	6.6	GGA
		(13.107	3.743	152.4	5.0)[a]	
		12.075	3.642	193.6	7.2	LDA
		(12.052	3.640	197.1	4.8)[a]	
		(13.184	3.750)[c]			Exp.
Ni_7In_3	aP40	13.826	11.147, 11.129, 6.600 126.37°, 61.35°, 119.47°	138.3	6.6	GGA
		12.718	10.847, 10.838, 6.415 126.45°, 61.58°, 118.89°	173.6	6.4	LDA
		13.606	11.098, 11.097, 6.572[d] 126.59°, 61.15°, 119.58°			Exp.
Ni_2In	hP6	14.158	4.314, 5.271	143.6	6.1	GGA
		(14.183	4.317, 5.273	135.9	2.9)[a]	
		(13.556	4.265, 5.163)[c]			
		12.967	4.193, 5.110	171.9	6.5	LDA
		(12.980	4.196, 5.106	174.4	5.0)[a]	
Ni_5In_3	mC32	14.793	12.549, 7.207, 6.658, 51.83°	124.3	7.3	GGA
		13.625	12.207, 7.015, 6.479 51.80°	162.0	5.8	LDA
$Ni_{13}In_9$	mC44	15.078	14.862, 8.464, 9.120 35.33°	131.4	5.0	GGA
		13.839	14.448, 8.220, 8.860 35.36°	157.4	5.6	LDA
		(14.400	14.646, 8.329, 8.977 35.35°)[c]			Exp.
NiIn	hP6	17.635	5.282, 4.379	99.5	7.7	GGA
		(17.571	5.274, 4.376	107	4.7)[a]	
		(17.683	5.287, 4.383	102)[e]		
		(16.230	5.139, 4.257	131.9	5.1)	LDA)[a]
		(16.192	5.130, 4.267	132.1	5.1)[a]	
		(17.267	5.244, 4.350	153	4.0)[f]	Exp.
Ni_2In_3	hP5	18.278	4.443, 5.345	94.5	5.8	GGA
		(18.277	4.453, 5.321	93.2	5.1)[a]	
		16.786	4.314, 5.207	121.2	6.0	LDA
		(16.708	4.306, 5.203	123.1	5.5)[a]	
		(17.358	4.390, 5.200)[c]			Exp.[c]
Ni_3In_7	cI40	20.090	9.297	77.1	6.7	GGA
		18.377	9.025	102.0	6.1	LDA
		(19.340	9.180)[c]			Exp.

[a] Ferromagnetic (FM) FP-LAPW GGA-PBE and LDA-PW calculations including relaxations of internal coordinates [17].
[b] FM FP-LAPW GGA-PBE calculations (without relaxations of internal coordinates) [12,13].
[c] Experimental data [8].
[d] Experimental data [10,11].
[e] PAW GGA-PW91 [18].

B_o show larger discrepancies with experiments, and the GGA calculated values are closer to the experimental ones than those given by the LDA. Specifically, the GGA underestimates B_o, and the largest deviations amount to −16% for Sn and −13% for In. The LDA calculated B_o values are larger than the experimental ones. This correlates with the smaller LPs indicating that the LDA predictions show a typical overbinding effect. In particular, deviations of up to 38% are obtained in the case of Ni. Acceptable agreement with experimental values (*i.e.* within 31%) is obtained for the B'_o. The present B_o and B'_o are also in good agreement with other reported values from US-PP [31] (for B_o, within 3% for LDA and 6% for GGA) and FP-LAPW (for B_o, less than 2% for LDA and 8% for GGA) [17] calculations. It should be mentioned that no significant differences are found between the present spin-polarized results for In and Sn and those obtained in our previous work using a slightly lower value for the energy cut-off (314 eV) [32].

3.2. Structural and EOS parameters for Ni–In and Ni–Sn compounds

The structural and EOS parameters for the Ni–In and Ni–Sn compounds studied in the present work are listed in Tables 3 and 4, respectively, together with other information to be discussed in the following. The present values for the unit-cell internal coordinates of Ni–In and Ni–Sn compounds are given in Table 5. In Fig. 3 we compare the present GGA (circles) with the LDA (triangles) values for V_o and B_o for Ni–In (3a and c) and

Table 4
Structural and elastic properties for Ni–Sn intermetallic phases at 0 K. The lattice parameters are given in Å, the equilibrium volume (V_o) in Å^3/atom, the bulk modulus (B_o) in GPa.

Phase	PS	V_o	a, b, c, α, β, γ	B_o	B'_o	Aprox.
Stable						
Ni_3Sn	hP8	13.021	5.317, 4.255	166.7	6.3	GGA
		(13.106	5.326, 4.268	162.0	5.1)[a]	
		12.065	5.181, 4.153	209.4	5.7	LDA
		(12.104	5.185, 4.137	204.8	4.8([a]	
		(12.890	5.295, 4.247)[b]			
Ni_3Sn	cF16	13.086	5.938	162.0	6.0	GGA
		(13.179	5.952	161.2	5.2)[a]	
		12.108	5.786	204.1	6.0	LDA
		(12.170	5.7961	203.6	4.7)[a]	
		(13.379	5.982)[c]			
Ni_3Sn_2	oP20	15.381	7.164, 5.228, 8.213	132.1	5.7	GGA
		(15.473	7.185, 5.234, 8.226	128.1	4.9)[a]	
		14.217	6.985, 5.094, 7.991	164.2	4.4	LDA
		14.296	7.002, 5.100, 8.004	161.5	4.9[a]	
		(15.091	7.125, 5.195, 8.154)[d]			
Ni_3Sn_4	mC14	18.304	12.312, 4.087, 5.266 104.78°	101.8	3.0	GGA
		(18.460	12.324, 4.110, 5.284 105.1°	96.7	5.0)[a]	
		16.971	12.024, 3.988, 5.131 105.1°	127.5	5.7	LDA
		(17.032	12.013, 4.000, 5.145 105.3	123.0	4.9)[a]	
		(18.104	12.215, 4.060, 5.291) 105.0°[c]			
Metastable						
Ni_3Sn	cP4	13.030	3.735	163.6	5.8	GGA
		(13.120	3.744	163.4	4.9)[a]	
		12.055	3.640	208.5	6.4	LDA
		(12.116	3.646	204.5	4.7)[a]	
		(13.057	3.738)[c]			
$NiSn_4$	oC20	23.433	6.341, 6.383, 11.579	57.5	6.4	GGA
		(23.558	6.347, 6.369, 11.660	55.5	4.7)[a]	
		21.577	6.177, 6.218, 11.236	73.7	6.6	
		(21.623	6.171, 6.199, 11.296	7.3	5.4)[a]	LDA
		(23.392	6.397, 6.426, 11.381)[e]			

[a] *Ab initio* US-PP [31].
[b] Ref. [61].
[c] Ref. [8].
[d] Ref. [26].
[e] Ref. [29].

Ni–Sn (3b and d) and with the experimental data for V_o (crosses). The dashed lines are only to guide the eye. In Fig. 4, the present GGA (filled circles) and LDA (filled triangles) for V_o (4a and b) and B_o (4c and d) for Ni–Sn compounds are compared with the results by Ghosh [31] using GGA (empty circles), LDA (empty triangles) and with experiments (crosses).

In most of the cases, the GGA values for the LPs of Ni–In and Ni–Sn deviate positively from experiments, with a difference less than 3%. Some negative deviations which are smaller in magnitude are also observed. The corresponding LDA values are smaller than the experimental ones by less than 3.5%. Concerning B_o and B'_o, we remark that a comparison with experiments is possible only for NiIn (hP6). In this case the LDA leads to deviations of 14% and 27%, respectively, whereas the GGA differences are about 3 times larger. Similar GGA calculations [18] give comparable deviations for B_o. In general, for Ni–In compounds, the typical differences for B_o between the present and the FP-LAPW LDA and GGA results [17] are less than 2%, except for Ni_2In (hP6) where the difference amounts at 6%.

According to Fig. 3 the GGA calculations slightly overestimate V_o of most of the stable Ni–In and Ni–Sn compounds, as found for other systems (see, *e.g.*, Refs. [46,47]), whereas the LDA calculated V_o values are systematically smaller than the experimental ones with a more important discrepancy. A similar behavior has been found for other intermetallic systems [17,31,48]. Also in accord with the expected trends, the theoretical B_o values for Ni–In (Fig. 3c) and Ni–Sn (Fig. 3d) compounds obtained with the GGA are smaller than those obtained with the LDA. The comparisons in Fig. 4 indicate that similar trends in the comparison with experiments emerge from the US-PP results by Ghosh [31] using LDA and GGA calculations.

The present results for Ni–In and Ni–Sn indicate a smooth variation of V_o and B_o with composition. In particular, the *ab initio* calculated V_o values for the Ni–In and Ni–Sn compounds deviate negatively from those that would yield a linear interpolation between the results for the elements. For B_o, negative deviations are suggested by the LDA results, whereas the GGA values show smaller deviations of both signs. The present results support the observation that a negative deviation from linearity in the composition dependence in V_o (or B_o) does not necessarily imply a positive deviation in B_o (or V_o), as generally expected [31].

3.3. Electronic and magnetic properties of intermetallic phases

In this section we discuss the electronic and magnetic properties of some selected Ni–In and Ni–Sn IPs. In particular, we focus

Table 5
Unit cell internal coordinates of Ni_3In, Ni_7In_3, Ni_5In_3, $Ni_{13}In_9$, Ni_2In_3, Ni_3In_7, Ni_3Sn, Ni_3Sn_2, Ni_3Sn_4 and $NiSn_4$ calculated *ab initio* in the present work and experimental data [8,11].

Phase	Site	Internal coordinates		
		(*x*, *y*, *z*): Calculated	(*x*, *y*, *z*): Calculated	(*x*, *y*, *z*): Exp.
Ni–In		GGA	LDA	
Ni_3In	Ni:6h	0.844, 0.688, 0.250	0.844, 0.687 0.250	0.833, 0.666, 0.250[a]
	In:2c	0.333, 0.666, 0.250	0.333, 0.666, 0.250	0.333, 0.666, 0.250
Ni_7In_3	Ni:1a	0.000, 0.000, 0.000	0.000, 0.000, 0.000	0.000, 0.000, 0.000[b]
	Ni:2i	0.303, 0.458, 0.005	0.303, 0.458, 0.005	0.295, 0.454, 0.001
	Ni:2i	0.134, 0.713, 0.017	0.134, 0.713, 0.018	0.134, 0.711, 0.013
	Ni:2i	0.420, 0.147, 0.999	0.420, 0.147, 0.999	0.419, 0.146, 0.996
	Ni:1d	0.500, 0.000, 0.500	0.500, 0.000, 0.500	0.500, 0.000, 0.500
	Ni:2i	0.936, 0.146, 0.506	0.936, 0.146, 0.506	0.932, 0.144, 0.514
	Ni:2i	0.224, 0.576, 0.502	0.224, 0.576, 0.502	0.231, 0.575, 0.495
	Ni:2i	0.352, 0.302, 0.500	0.352, 0.302, 0.500	0.348, 0.301, 0.483
	Ni:2i	0.163, 0.002, 0.162	0.163, 0.002, 0.165	0.162, 0.001, 0.166
	Ni:2i	0.664, 0.144, 0.240	0.664, 0.144, 0.240	0.663, 0.143, 0.239
	Ni:2i	0.750, 0.982, 0.260	0.750, 0.982, 0.260	0.749, 0.982, 0.258
	Ni:2i	0.284, 0.766, 0.343	0.284, 0.765, 0.341	0.283, 0.762, 0.335
	Ni:2i	0.438, 0.455, 0.262	0.438, 0.456, 0.264	0.440, 0.458, 0.266
	Ni:2i	0.864, 0.589, 0.251	0.864, 0.589, 0.252	0.866, 0.584, 0.248
	Ni:2i	0.915, 0.232, 0.248	0.916, 0.233, 0.247	0.918, 0.236, 0.248
	In:2i	0.056, 0.527, 0.256	0.056, 0.527, 0.257	0.056, 0.534, 0.269
	In:2i	0.365, 0.996, 0.251	0.365, 0.997, 0.251	0.370, 0.992, 0.258
	In:2i	0.513, 0.710, 0.261	0.513, 0.710, 0.261	0.520, 0.711, 0.268
	In:2i	0.186, 0.267, 0.234	0.187, 0.267, 0.233	0.170, 0.267, 0.218
	In:2i	0.895, 0.840, 0.273	0.895, 0.839, 0.272	0.895, 0.846, 0.277
	In:2i	0.627, 0.365, 0.215	0.628, 0.365, 0.213	0.633, 0.372, 0.216
Ni_5In_3	Ni:4c	0.089, 0.149, 0.249	0.090, 0.148, 0.249	
	Ni:4c	0.410, 0.186, 0.251	0.410, 0.187, 0.251	
	Ni:4c	0.750, 0.167, 0.250	0.750, 0.167, 0.250	
	Ni:4c	0.172, 0.998, 0.494	0.172, 0.998, 0.494	
	Ni:4c	0.323, 0.333, 0.006	0.328, 0.333, 0.006	
	In:2a	0.000, 0.034, 0.000	0.000, 0.034, 0.000	
	In:2b	0.000, 0.800, 0.500	0.000, 0.800, 0.500	
	In:4c	0.358, 0.982, 0.986	0.359, 0.982, 0.986	
	In:4c	0.142, 0.352, 0.513	0.142, 0.353, 0.514	
$Ni_{13}In_9$	Ni:2c	0.000, 0.000, 0.500	0.000, 0.000, 0.500	0.000, 0.000, 0.500[a]
	Ni:4f	0.250, 0.250, 0.500	0.250, 0.250, 0.500	0.250, 0.250, 0.500
	Ni:4g	0.000, 0.263, 0.000	0.000, 0.265, 0.000	0.000, 0.248, 0.000
	Ni:4i	0.260, 0.000, 0.000	0.260, 0.000, 0.001	0.248, 0.000, 0.010
	Ni:4i	0.453, 0.000, 0.269	0.454, 0.000, 0.270	0.445, 0.000, 0.275
	Ni:8j	0.804, 0.258, 0.732	0.804, 0.259, 0.732	0.807, 0.251, 0.731
	In:2d	0.000, 0.500, 0.500	0.000, 0.500, 0.500	0.000, 0.500, 0.500
	In:4i	0.709, 0.000, 0.748	0.710, 0.000, 0.746	0.701, 0.000, 0.762
	In:4i	0.176, 0.000, 0.765	0.175, 0.000, 0.765	0.172, 0.000, 0.760
	In:8j	0.960, 0.211, 0.7771	0.960, 0.210, 0.7771	0.957, 0.227, 0.768
Ni_2In_3	Ni:2d	0.333, 0.666, 0.141	0.333, 0.666, 0.141	0.333, 0.666, 0.135[a]
	In:1a	0.000, 0.000, 0.000	0.000, 0.000, 0.000	0.000, 0.000, 0.000
	In:2d	0.333, 0.666, 0.646	0.333, 0.666, 0.646	0.333, 0.666, 0.641
Ni_3In_7	Ni:12e	0.355, 0.000, 0.000	0.355, 0.000, 0.000	0.335, 0.000, 0.000[a]
	In:12d	0.250, 0.000, 0.500	0.250, 0.000, 0.500	0.250, 0.000, 0.500
	In:16f	0.161, 0.161, 0.161	0.161, 0.161, 0.161	0.159, 0.159, 0.159
Ni–Sn				
Ni_3Sn	Ni:6h	0.841, 0.688, 0.250	0.841, 0.681 0.250	0.833, 0.666, 0.250[a]
	In:2c	0.333, 0.666, 0.250	0.333, 0.666, 0.250	0.333, 0.666, 0.250
Ni_3Sn_2	Ni:4c	0.908, 0.250, 0.128	0.908, 0.250, 0.127	0.909, 0.250, 0.127[a]
	Ni:8d	0.236, 0.004, 0.876	0.235, 0.004, 0.876	0.240, 0.006, 0.877
	Sn:4c	0.607, 0.250, 0.596	0.607, 0.250, 0.596	0.593, 0.250, 0.647
	Sn:4c	0.560, 0.250, 0.096	0.561, 0.250, 0.096	0.576, 0.250, 0.128
Ni_3Sn_4	Ni:2a	0.000, 0.000, 0.000	0.000, 0.000, 0.000	0.000, 0.000, 0.000[a]
	Ni:4i	0.215, 0.000, 0.336	0.216, 0.000, 0.336	0.215, 0.000, 0.337
	Sn:4i	0.428, 0.000, 0.688	0.427, 0.000, 0.688	0.429, 0.000, 0.686
	Sn:4i	0.172, 0.000, 0.812	0.171, 0.000, 0.811	0.172, 0.000, 0.812
$NiSn_4$	Ni:4a	0.000, 0.000, 0.000	0.000, 0.000, 0.000	0.000, 0.000, 0.000
	Sn:8b	0.177, 0.324, 0.123	0.176, 0.326, 0.123	0.173, 0.327, 0.125
	Sn:8b	0.323, 0.176, 0.877	0.324, 0.174, 0.877	0.327, 0.173, 0.875

[a] Ref. [8].
[b] Ref. [11].

on the effect upon the electronic density of states (DOS) of the changes in the In (or Sn) content. In Fig. 5 we plot the GGA calculated DOS for the Ni_3In (hP8), NiIn (hP6) and Ni_3In_7 (cI40) phases of the Ni–In system, and in Fig. 6 the results for the Ni_3Sn (hP8),

Table 6
Total and site decomposed density of states at the Fermi level $N(E_F)$ (in units of states/eV/f.u.) of Ni_3In and Ni_3Sn, in the hP8 structures. I (in units of eV) denotes the Stoner parameter. NM and FM denote the nonmagnetic and ferromagnetic states, respectively.

Fases	SP	$N_t\ (E_F)$	$N_{In,Sn}\ (E_F)$	$N_{Ni\text{-}d}\ (E_F)$	I (eV)	$N_t\ (E_F)I$
Ni_3In-NM	hP8	9.1765	0.1233	2.8513	0.1457	1.337
FM-UP		0.6992	0.0605	0.1751		
FM-DN		4.7739	0.0993	1.4711		
Ni_3Sn-NM	hP8	2.2706	0.1520	0.6085	0.1084	0.246
FM-UP		1.1239	0.0722	0.2281		
FM-DN		1.1239	0.0722	0.2281		

Ni_3Sn_2(oP20) and $NiSn_4$(oC20) phases of the Ni–Sn system. The partial DOS of the Ni-4s and Ni-3d electrons as well as for the In/Sn-5s and In/Sn-5p are also plotted.

In the first place, we discuss some common features and differences of the DOS of the Ni–In and Ni–Sn phases treated here, for which not only their In/Sn composition changes but also their structures do. Therefore both composition and structural changes will affect in the resulting shape of the DOS. The DOS is dominated by a Ni-3d band extending between the Fermi level, which falls on the upper edge of the band, and 3 eV below. For the compounds with higher In/Sn content the Ni-3d bands are slightly narrower and are shifted to lower energies with respect to the Fermi level,

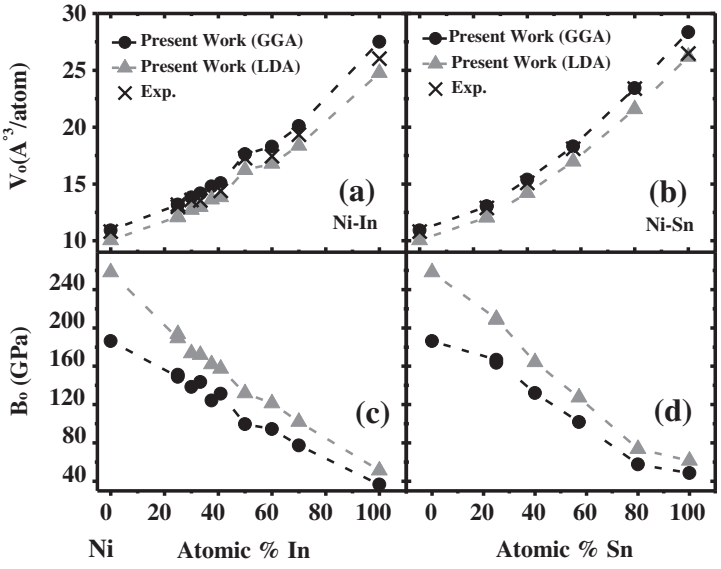

Fig. 3. Thermophysical properties of the Ni–In and Ni–Sn intermetallic phases calculated in the present work as functions of the atomic composition of In and Sn: (a and b) volume (V_o) per atom; (c and d) bulk modulus (B_o). Filled symbols correspond to values calculated in this work using GGA (circles) and LDA (triangles). Crosses correspond to experimental values [8]. The dashed lines are only guides to the eye.

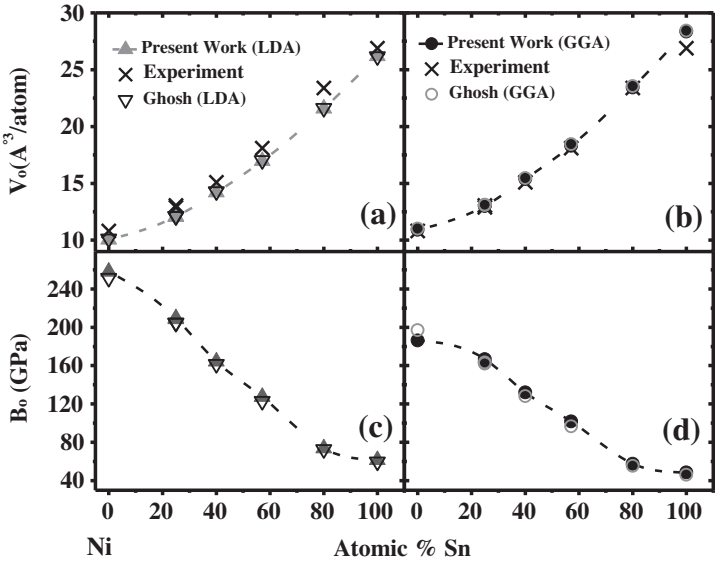

Fig. 4. Thermophysical properties of the Ni–Sn intermetallic phases calculated in the present work as functions of the atomic composition of In and Sn, compared with the *ab initio* US-PP results of Ghosh [31]: (a and b) volume (V_o) per atom; (c and d) bulk modulus (B_o). Filled symbols correspond to values calculated in this work using GGA (circles) and LDA (triangles). Empty symbols correspond to the US-PP values calculated in Ref. [31] and crosses correspond to experimental values [8]. The dashed lines are only guides to the eye.

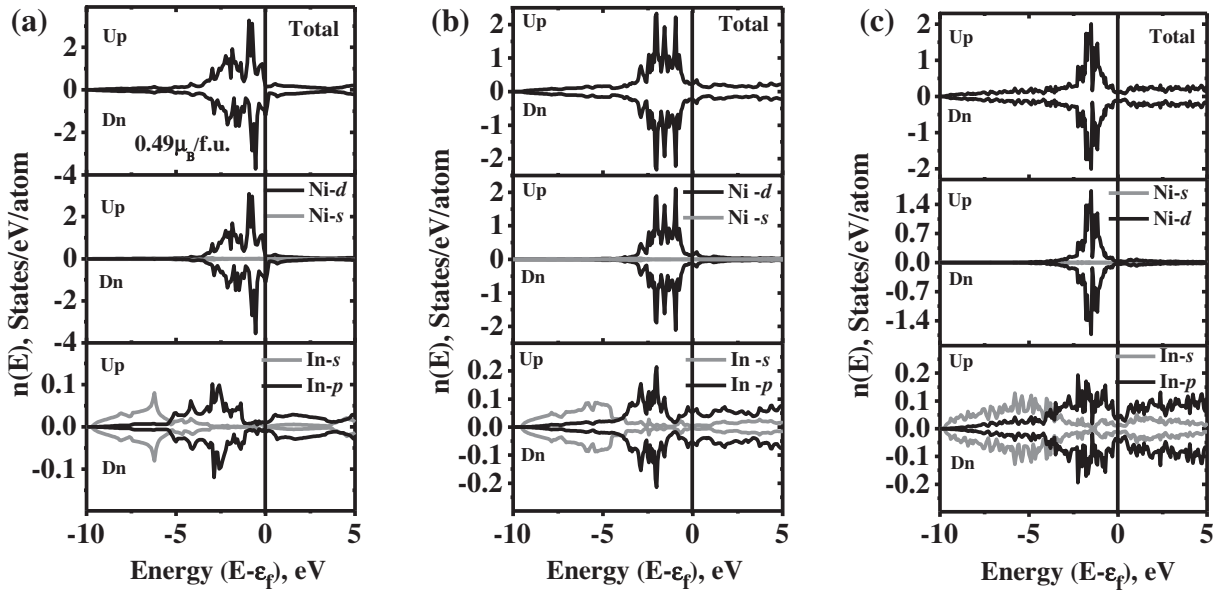

Fig. 5. Total and partial electronic density of states (DOSs) for Ni–In compounds: (a) Ni_3In-hP8, (b) NiIn-hP6 and (c) Ni_3In_7-cI40. The partial DOS of the Ni-4s and Ni-3d electrons as well as for the In-5s and In-5p are also plotted. The origin of the energy scale corresponds to the Fermi level.

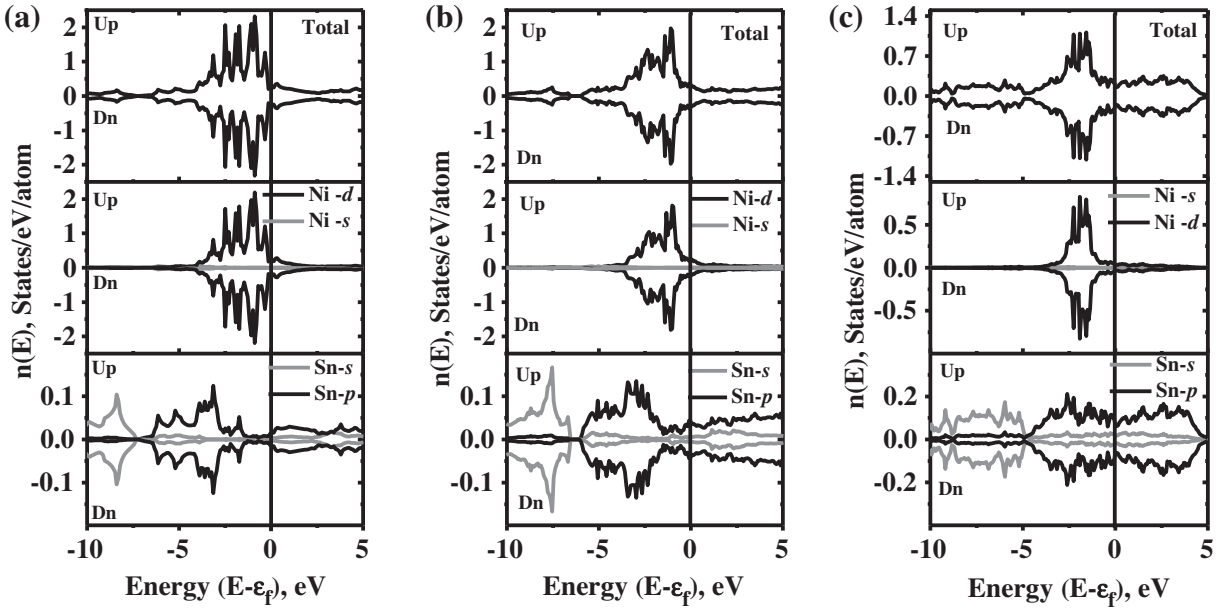

Fig. 6. Total and partial electronic density of states (DOSs) for Ni–Sn compounds: (a) Ni_3Sn-hP8, (b) Ni_3Sn_2-oP20 and (c) $NiSn_4$-oC20. The partial DOS of the Ni-4s and Ni-3d electrons as well as for the Sn-5s and Sn-5p are also plotted. The origin of the energy scale corresponds to the Fermi level.

as compared with the compounds with lower In/Sn content. There is mixing of the Ni-3d band with the broad free-electron-like In/Sn-5p band with a minor contribution of In/Sn-5s states. At lower energies the free-electron type contribution of the In/Sn-5s electrons dominates, increasing their importance for the compounds at higher In/Sn content. The DOS per atom (given in states eV^{-1}-$atom^{-1}$) at the Fermi level is relatively low but finite in all cases, indicating metallic character of the studied Ni–In and Ni–Sn IPs. Below −3 eV approximately the main contribution to the DOS comes mainly from dispersive Ni-s and In/Sn-s/p states. Above the Fermi level, the bands are extended and result from the hybridization between Ni-3d and In/Sn-5p orbitals. The contributions of the Ni-4s and In/Sn-5s electrons to the conduction band are negligibly small. The total occupied (conduction) bandwidth is 10 eV approximately.

Second, we compare the electronic behavior of the Ni–In and Ni–Sn systems by focusing on the DOS of Ni_3In and Ni_3Sn (Figs. 5a and 6a), *i.e.*, two compounds with the same formula and structure (hP8). It is observed that the Ni-3d and In/Sn-5p hybridization effect is stronger for the Ni–Sn phase. This might be related to the fact that Sn has a larger number of p electrons (4) than In (3). In turn, this stronger hybridization effect, and the associated stronger bonding, might be correlated with the larger values for B_o and the relatively higher thermodynamic stability (measured by the

Table 7
Energy of formation ($\Delta_f E$) (in kJ/mol-atom) for Ni–In intermetallic phases obtained by *ab initio* calculations at 0 K, Calphad assessments [34] and experiments [62] at 298.15 K. Reference states are Ni (fcc) and In (tI2).

Phase	PS	*Ab Initio* $\Delta_f E$		$\Delta_f E$	$\Delta_f E$
Ni–In		PAW-LDA	PAW-GGA	Calphad assessments	Experimental
Stable					
Ni3In	hP8	−11.702	−8.182	−13.116	−11.732
		−10.309[a]	−6.326[a]		
Ni3In	cP4	−9.604	−5.921		
		−7.964[a]	−4.232[a]		
Ni7In3	aP40	−14.450	−10.392		
Ni2In	hP6	−9.012	−4.703	−16.381	−17.339
		−5.992[a]	−1.432[a]		
Ni5In3	mC32	−17.961	−13.158		
Ni13In9	mC44	−18.816	−13.846	−19.157	
NiIn	hP6	−25.224	−20.808	−22.531	−23.681
		−23.148[a]	−17.517[a]		
Ni2In3	hP5	−24.426	−17.951	−25.603	−20.718
		−22.434[a]	−15.441[a]		
Ni3In7	cI40	−20.689	−15.194	−19.751	−17.681

[a] FM FP-LAPW GGA-PBE and LDA-PW calculations including relaxations of internal coordinates [17].

Table 8
Energy of formation ($\Delta_f E$) (in kJ/mol-atom) for Ni–Sn intermetallic phases obtained by *ab initio* calculations at 0 K, Calphad assessments (data at 298.15 K) and experiments. Reference states are Ni (fcc) and Sn (tI4).

Phase	PS	*Ab Initio* $\Delta_f E$		$\Delta_f E$	$\Delta_f E$
Ni–Sn		PAW-LDA	PAW-GGA	Calphad assessments	Experimental
Stable					
Ni_3Sn	hP8	−24.157	−19.627	−26.882[b]	−23.442[e]
		−23.452[a]	−18.052[a]	−26.657[c]	−24.400[f]
Ni_3Sn	cF16	−19.119	−15.324	−21.745[b]	−21.000[f]
		−17.787[a]	−13.253[a]	−26.538[c]	
Ni_3Sn_2	oP20	−33.139	−27.781	−36.989[d]	−38.500[g]
		−31.758[a]	−25.994[a]		
Ni_3Sn_4	mC14	−29.427	−24.857	−26.138[b]	−25.330[h]
		−28.155[a]	−23.279[a]	−25.409[c]	−24.000[i]
Metastable					
Ni_3Sn	cP4	−23.986	−19.679		
		−23.366[a]	−18.206[a]		
$NiSn_4$	oC20	−13.985	−12.480		
		−13.460[a]	−11.819[a]		

[a] Ref. [31].
[b] Ref. [35].
[c] Ref. [63].
[d] Ref. [64].
[e] Ref. [66].
[f] Ref. [65].
[g] Ref. [67].
[h] Ref. [68].
[i] Ref. [69].

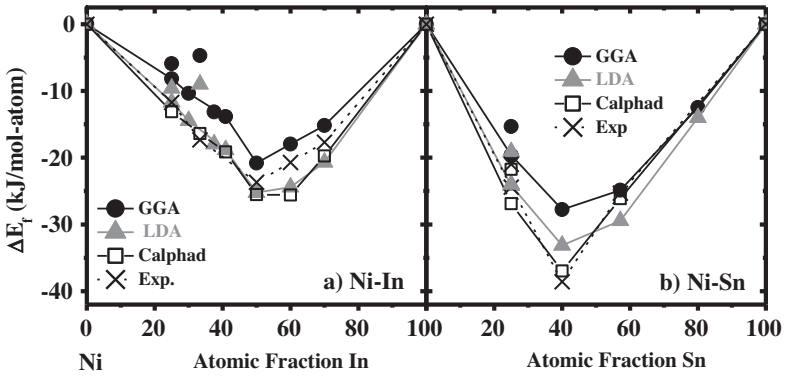

Fig. 7. Composition dependence of the energy of formation (EOF) from the elements of the Ni–In (a) and Ni–Sn (b) stable and metastable compounds studied in the present work. Filled symbols correspond to values calculated in this work using GGA (circles) and LDA (triangles). Empty squares correspond to values obtained in the CALPHAD assessments of Waldner and Ipser for Ni–In [34] and Liu et al. for Ni–Sn [35]. Crosses represent experimental data from the references listed in Tables 7 and 8.

Table 9
Ab initio EOF of the end-member-compounds (EMC) corresponding to the thermodynamic sublattice models proposed for Ni–In [34] and Ni–Sn [35] phases. In the first column we indicate the phase, the model and the Wyckoff crystallographic positions chosen for each crystallographic sublattice. When more than one possibility exists the results are indicated on the left and right of the corresponding row. In the last column we indicate the differences between the 0 K *ab initio* and CALPHAD (at 298.15 K) results. The *ab initio* EOF are referred to Ni (fcc) in the magnetic state. The values referred to Ni (fcc) in the paramagnetic state are indicated in italics.

Phase (Pearson symbol) Sublattice model Subl. Wyckoff positions	Sublattice occupation scheme	EMC formula	Energy of formation (kJ/mol)				
			Present Study		CALPHAD work	Difference	
ζ-Ni_2In (hP6) $(Ni)_1(Ni,Va)_1(In)_1$ (2a; 2d; 2c)	Ni:Ni:In	"Ni_2In"	−4.70		−16.31	+11.61	
			−7.92			*+8.39*	
	Ni:Va:In	"NiIn"	−7.22		−13.30	+6.08	
			−9.64			*+3.66*	
	Ni:Ni:Ni	"Ni_3"	+11.75		+17.56	−5.79	
			+6.91			*−10.63*	
	Ni:Va:Ni	"Ni_2"	+49.98		+17.56	+32.42	
			+45.13			*+27.57*	
ζ'-$Ni_{13}In_9$ (hP6) $(Ni)_1(Ni,Va)_1(In)_1$ (2a; 2d; 2c)	Ni:Ni:In	"Ni_2In"	−4.70		−16.37	+11.67	
			−7.92			*+8.45*	
	Ni:Va:In	"NiIn"	−7.22		−22.50	+15.28	
			−9.64			*+12.86*	
δ-NiIn (B2) $(Ni,Va)_1(In)_1$ (1b; 1a)	Ni:In	"NiIn"	−10.17		−16.74	+6.57	
			−12.59			*+4.15*	
	Ni:Ni	"Ni_2"	+9.09		+8.71	+0.38	
			+4.25			*−4.46*	
	Va:In	"In"	+8.37		+43.04	−34.67	
	Va:Ni	"Ni"	+64.84		+171	−106.16	
			+60.00			*−111*	
Ni_3Sn_HT (cF16) $(Ni,Sn)_1(Ni,Sn)_1(Ni)_2$ (4a; 4b; 8c)	Ni:Ni:Ni	"Ni_4"	+8.38		0	+8.38	
			+3.53			*+3.53*	
	Ni:Sn:Ni	"Ni_3Sn"	−15.12		−21.74	+6.62	
			−18.75			*+2.99*	
	Sn:Ni:Ni	"$SnNi_3$"	−15.13		+13.56	−28.69	
			−18.76			*−32.32*	
	Sn:Sn:Ni	"SnNi"	−0.70		−24.07	+23.37	
			−3.12			*+20.95*	
Ni_3Sn_2_LT (oP20) $(Sn)_1(Ni,Sn)_2(Ni)_2$ ($4c_{Sn1}$; $4c_{Sn2}$ + $4c_{Ni1}$; $8d_{Ni2}$) ($4c_{Sn2}$; $4c_{Sn1}$ + $4c_{Ni1}$; $8d_{Ni2}$)	Sn:Sn:Ni	"Sn_3Ni_2"	−9.01		−12.29	+3.28	
			−10.95			*+1.34*	
	Sn:Ni:Ni	"$SnNi_4$"	+2.44	+2.38	−8.26	+10.70	+10.64
			−1.43	*−1.50*		*+6.83*	*+6.76*
Ni_3Sn_2_HT (hP6) $(Ni)_1(Ni,Sn)_1(Sn)_1$ (2a; 2d; 2c) (2d; 2a; 2c)	Ni:Ni:Sn	"Ni_2Sn"	−17.39		−22.45	+5.06	
			−20.62			*+1.83*	
	Ni:Sn:Sn	"$NiSn_2$"	+49.48	+19.40	−4.94	+54.42	+24.34
			+47.87	*+17.79*		*+52.81*	*+22.73*
Ni_3Sn_4 (mC16) $(Ni)_1(Ni,Sn)_1(Sn)_2$ ($4i_{Ni3}$;$2a_{Ni1}$ + $2c_{Ni2}$;$4i_{Sn1}$ + $4i_{Sn2}$) ($2a_{Ni1}$ + $2c_{Ni2}$;$4i_{Ni3}$;$4i_{Sn1}$ + $4i_{Sn2}$)	Ni:Ni:Sn	"NiSn"	−25.61		−26.14	+0.53	
			−28.03			*−1.89*	
	Ni:Sn:Sn	"$NiSn_3$"	−4.61	−2.85	+7.61	−12.22	−10.46
			−5.82	*−4.07*		*−13.43*	*−11.68*

magnitude of the EOF, see below) of Ni_3Sn compared with Ni_3In. It is also observed that the main Ni-3d band is wider for Ni_3Sn than for the Ni_3In compound, which might be correlated with the larger nearest neighbor distances of the latter, as reflected in the larger atomic volume, *viz.*, 13.188 Å^3/atom found for Ni_3In compared with 13.021 Å^3/atom for Ni_3Sn. The total DOS at the Fermi level for Ni_3Sn (0.56 states/eV/atom) is lower than for Ni_3In (1.37 eV/states/atom), a fact that correlates with the paramagnetic behavior predicted for this compound, as discussed below in terms of the Stoner criterion. It should be remarked that Ni_3In is the only IP among all Ni–In and Ni–Sn phases studied here that shows a permanent magnetic moment; its value being 0.49 μ_B/f.u. This result might be explained by applying the Stoner criterion for itinerant magnetism and its multiband extension to compounds [49,50]. This approach neglects the effects of localized, fluctuating moments, which may be present in this system. According to this theory the magnetic susceptibility becomes ferromagnetically unstable when $N_t(E_F)I > 1$, with $N_t(E_F)$ given by the total density of states per unit cell of the non-magnetic solution at the Fermi level, and I the Stoner parameter for the compound, given by:

$$I = \sum_j n_j I_j, I_j = \sum_l [N_l(E_F)/N_t(E_F)]^2 J_l$$

where $N_l(E_F)$ is the l partial density of states per atom at the Fermi level, and J_l the exchange integral for l orbitals, n_j the number of atoms of type j in the unit cell. Since the magnetism in the Ni–In/Sn

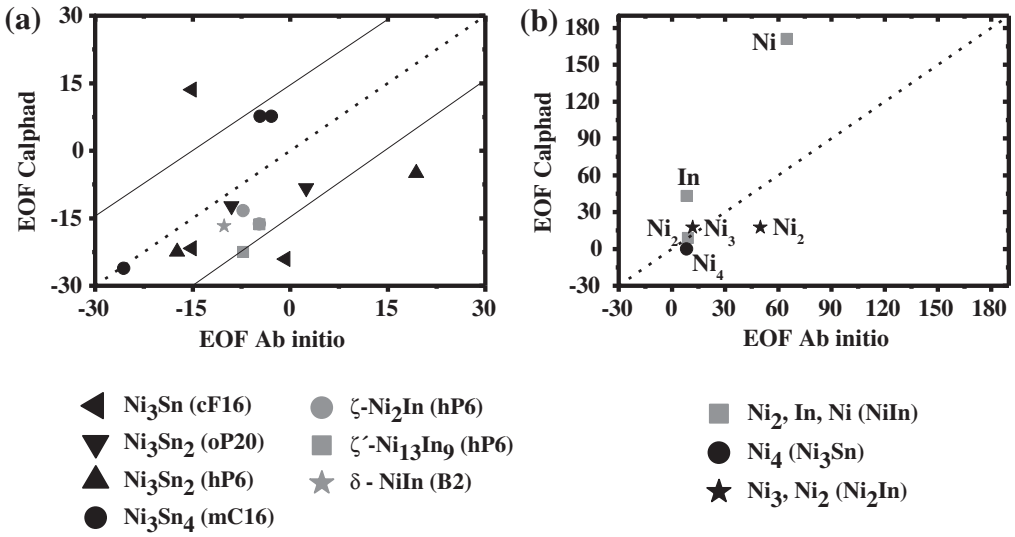

Fig. 8. Comparison between the *ab initio* and CALPHAD energy-of-formation (EOF) values for: (a) the Ni–In and Ni–Sn end-member-compounds involved in the thermodynamic models presented in Ref. [34] and [35], respectively; (b) the Ni–In and Ni–Sn end-members representing non-stable structures of the elements Ni, In and Sn. The EOF values are given in kJ/mol.

compounds is dominated by the 3d electrons of Ni, only these are considered to evaluate the Stoner parameter *I*. The exchange integral J_I for the Ni-3d electrons is 0.503 eV [49] and as a first approximation it is considered as independent of the crystalline structure and specific compound. In Table 6 we present the calculated Stoner factors for the Ni_3In and Ni_3Sn hP8 compounds. The Stoner factor is >1 for Ni_3In but <1 for Ni_3Sn. The ferromagnetic instability predicted for the Ni_3In compound might be related to its larger DOS at the Fermi level. For the remainder of the IPs studied here the DOS at the Fermi level has a relatively lower value, which is consistent with the fact that they are found to be paramagnetic.

3.4. EOF of stable and metastable stoichiometric compounds

The EOF of the stable and metastable Ni–In and Ni–Sn compounds studied in the present work are listed in Tables 7 and 8, respectively, together with other information to be discussed in the following. In Fig. 7 the composition dependence of the EOF of the Ni–In (7a) and Ni–Sn (7b) compounds, according to the present GGA (circles) and the LDA (triangles) 0 K calculations, is compared with experimental data (crosses) and with the values obtained in CALPHAD assessments (empty squares) at 298.15 K.

In agreement with the fact that Ni_3In, Ni_2In, $Ni_{13}In_9$, NiIn, Ni_2In_3 and Ni_3In_7 occur as stable low-temperature phases in the accepted equilibrium diagram, they are found to be thermodynamically stable with respect to the elements Ni and In (Fig. 7a). Concerning the Ni_3In compound and the relative stability between the hP8 and cP4 structures, we find in GGA and LDA calculations where the internal coordinates are allowed to relax, that the hP8 structure is more stable than the cP4 one by approximately 2 kJ/mol. This result agrees with experiments and a previous *ab initio* study [17]. When the internal coordinates are fixed at the experimentally reported positions [8] we find, in agreement with [13], that the relative stability is reversed, and the cP4 structure is predicted as more stable than the hP8, with an energy difference of 0.8 kJ/mol. The present study also indicates that the compounds Ni_7In_3 and Ni_5In_3, which are not included in the accepted phase diagram but have been detected around the Ni_2In composition range are thermodynamically stable with respect to the elements at 0 K. The Ni_3Sn, Ni_3Sn_2, Ni_3Sn_4 phases occurring at low temperature in the Ni–Sn phase diagram, as well as the metastable $NiSn_4$ compound are found to be thermodynamically stable (Fig. 7b).

Contrasting with the satisfactory qualitative agreement concerning the phase occurrence systematics, differences are found in the present work between the *ab initio* calculated EOF at 0 K and the finite temperature experimental values reported in the Ni–In (Fig. 7a) and Ni–Sn (Fig. 7b) systems. In particular, for the Ni–In compounds, the GGA leads to positive differences between the calculated and the experimental EOF varying between 2.5 and 12.6 kJ/mol. When the LDA is adopted, positive and negative deviations are obtained but they decrease in magnitude with values up to 8.3 kJ/mol, which represent a significative improvement of the agreement with experiments. For the Ni–Sn compounds, the differences between the present *ab initio* EOF and the experimental ones are smaller in magnitude, *viz.*, the GGA yields positive differences up to 10.8 kJ/mol, which decrease in magnitude by about 5.4 kJ/mol when the LDA is adopted. It should be emphasized that similar trends both in the comparison between *ab initio* and experimental EOFs and between LDA and GGA values have been reported for related systems. Specifically, for the stable phases of the Cu–In system the present authors recently reported discrepancies of about 7.4 kJ/mol obtained with the GGA, which decreased to 4.9 kJ/mol when the LDA was adopted [32]. Moreover, the EOF for Ni–Sn and Pd–Sn intermetallics calculated by Ghosh using US-PP and LDA were more negative by up to 5.5 kJ/mol and 4 kJ/mol, respectively, than those obtained with US-PP and GGA [31].

In closing the present comparison of the *ab initio* EOF calculated at 0 K with experimental high-temperature data and with CALPHAD extrapolations at 298.15 K, we would like to emphasize that an even more accurate assessment of the discrepancy should take into account the effect of temperature upon the measured heats of formation. To this end, the temperature-dependent quantity ΔC_p which measures the variation in heat-capacity (C_p) associated to the formation of the IPs from the elements should be integrated between 0 and 298.15 K. Such correction might not be large, but also not small enough to be neglected. Unfortunately, there is a serious lack of C_p data for the present IPs, and no experimental information allowing an estimation of their low-temperature ΔC_p *vs.* T function was found in the present work. In fact, the most recent thermodynamic assessments of the Ni–In [34] and Ni–Sn [35] systems included C_p data only for the NiIn and LT Ni_3Sn phases in

the high-temperature range. For the remaining IPs the high-temperature C_p was estimated using Neuman–Kopp's rule which corresponds to assuming $\Delta C_p = 0$, *i.e.*, by assuming that the heat of fornation is independent of temperature. The use of *ab initio* methods to estimate low-temperature heat capacities of the Ni–In and Ni–Sn phase was beyond the scope of the present investigation, but will be the matter of a specific study by the present authors.

3.5. EOF of compounds involved in CALPHAD modeling of non-stoichiometric phases

In addition to the stable and metastable stoichiometric IPs various compounds involved in the CALPHAD modeling of Ni–In and Ni–Sn non-stoichiometric phases using the CEF [6] have been treated. In particular, *ab initio* calculations were performed for the EMC involved in the CEF treatment of the δ-NiIn, ζ-Ni_2In and ζ'-$Ni_{13}In_9$ phases of the Ni–In system [34] and the Ni_3Sn, Ni_3Sn_2, Ni_3Sn_4 phases of the Ni–Sn system [35]. In Table 9 we present the *ab initio* calculated EOF for the EMC referred to above. Since in CALPHAD work the EOFs are sometimes referred to the elements in a hypothetical non-magnetic state, in addition to the EOF for Ni compounds referred to pure magnetic Ni, the values corresponding to Ni in the paramagnetic state are also reported in Table 9 using italics. However, the following discussion will be based on the values referred to magnetic Ni. Some of the EMC included in Table 9 correspond to the elements Ni, In and Sn in various hypothetical crystal structures; these will be considered in Section 3.6. The remaining values presented in this Table represent binary Ni–In and Ni–Sn compounds. The present treatment of the EMC involved in the sublattice models proposed in Ref. [34] for phases of the Ni–In system, and in Ref. [35] for the Ni–Sn system, was based on correlating the thermodynamic-model sublattices of the CEF with the actual crystallographic sublattices defined by sites sharing the same symmetrical Wyckoff positions. In particular, for the three-sublattice models used in Ref. [34] to describe the Ni_2In and $Ni_{13}In_9$ phases, *viz.*, $(Ni)_1(Ni,Va)_1(In,Ni)_1$ and $(Ni)_1(Ni,Va)_1(In)_1$, respectively, we adopted the basic hP6 structure and identified the crystallographic sublattices comprising the Wyckoff sites 2a, 2d and 2c with the thermodynamic sublattices 1, 2 and 3, respectively, of the Gibbs energy models. For the other IPs considered in this section the details on how the symmetrical Wyckoff positions are assigned to each sublattice in the corresponding thermodynamic model are indicated in the first column of the Table 9. For the Ni_3Sn_4 we considered the alternative mC16 structure proposed in the literature [8], since for this structure it is easier to identify the crystallographic sublattices. In the Ni–Sn system there are phases like Ni_3Sn_2 (LT) (oP20), Ni_3Sn_2 (HT) (hP6) and Ni_3Sn_4 (mC16) for which we tested at least two possibilities for the selection of the sublattice sites; these are indicated in two different rows below each description of the sublattice model. The EOF corresponding to these alternatives are indicated on the left and right of the same row in Table 9. It should be recognized that other possibilities might exist for identifying the crystallographic sites with the thermodynamic sublattices. In this study we focussed upon those that are closer to the experimentally reported structure. In general, in those cases for which different crystallographic options were tested, the ones with the lower number of Sn-Sn bonds were the most stable. However, only for Ni_3Sn_2 (HT) (hP6) the difference between the energies for the two possible occupation alternatives was found to be significant. In particular, in one case, the sites 2a were chosen for the $(Ni,Sn)_1$ thermodynamic sublattice; in the other, this sublattice was identified with the sites 2d.

In the following the theoretical results are used to critically analyze various predictions and estimations for non-stable compounds produced by CALPHAD techniques. A first question concerns the quantitative agreement between the *ab initio* and CALPHAD EOF values for the EMC of the quoted Ni–In and Ni–Sn models. The comparison presented in Fig. 8a indicates that for most of the compounds the difference is less than ±15 kJ/mol. Two other issues of interest are the quantitative account of the structure dependence of the EOF and the effect of different sublattice occupation schemes upon the EOF for the non-stable phases. These two effects will be characterized by performing various comparisons based upon the results in Table 9.

Considering in the first place EMC with the same structure and formula, the CALPHAD method correctly yields almost the same EOF values for the "Ni_2In" compound originated by the sublattice occupation Ni:Ni:In involved in the CEF models for the ζ-Ni_2In (hP6) and ζ'-$Ni_{13}In_9$ (hP6) phases. However, for the "NiIn" compound with the (hP6) structure, generated by the sublattice occupation Ni:Va:In in the same CEF models, the CALPHAD optimization led to EOF differing by about 9.2 kJ/mol, *i.e.*, a significative energy difference. A second comparison concerns the *ab initio* and CALPHAD predictions for the EOF of Ni–In and Ni–Sn compounds with the same formula but different structure. According to Table 9, the EOF of the "NiIn" compound in the (hP6) and the B2 structure differ by about 3 kJ/mol, whereas the CALPHAD difference is 8 kJ/mol. Another case to analyze involves the "SnNi" (cF16) and the "NiSn" (mC16) compounds originated by the sublattice occupations Sn:Sn:Ni and Ni:Ni:Sn, respectively. The *ab initio* EOF of these two compounds differ by 25 kJ/mol, whereas the difference between the CALPHAD results is only 2 kJ/mol. The next comparisons concern compounds with the same formula but different sublattice occupation. The first case involves the "Ni_3Sn" and the "$SnNi_3$" EMC originated by the sublattice occupations Ni:Sn:Ni and Sn:Ni:Ni of the model for Ni_3Sn (HT) (cF16). The *ab initio* calculated EOF for these compounds are almost identical, whereas the CALPHAD approach yield values differing by more than 35 kJ/mol. A second case involves the "$NiSn_2$" phase originated in the Ni:Sn:Sn occupation scheme of the model for the Ni_3Sn_2 (HT) (hP6) phase. As stated before, calculations were performed in the present work for two alternative identifications of the thermodynamic with the actual crystallographic sublattices, which yield EOF values of about 20 and 50 kJ/mol, with reference to Ni in the magnetic sate. On the other hand, the CALPHAD optimization yields for this phase a single value, *viz.*, −5 kJ/mol, which is considerably smaller than both theoretical results.

3.6. Structural energy differences ("lattice-stabilities") for Ni and In

Motivated by the long-standing interest in the comparison between *ab initio* and CALPHAD-generated energy differences between the non-stable and stable structures (often called "lattice-stabilities" [5]) of the elements (see *e.g.*, Wang et al. [51] and references therein), we focus in the following upon the EOF for those EMC representing non-stable structures of the elements Ni and In. In the first place, a general comparison is presented in Fig. 8b between the *ab initio* (at 0 K) and CALPHAD (at 298.15 K) EOF values for these non-stable structures. Most of the CALPHAD generated values fall in a scatter band of ±35 kJ/mol around the *ab initio* results. Starting the discussion of such a difference, we remark, in the first place, that the magnitude of the scatter band in Fig. 8b is comparable to the differences found by Wang et al. [51] when comparing the PAW-GGA *ab initio* results for the lattice stabilities of the fcc, bcc and hcp structures of 78 pure elements and the CALPHAD generated values included in the SGTE database. They found differences of up to 50 kJ/mol for the stability difference between bcc and fcc [51]. In the second place we note that in the quoted CALPHAD works [34,35] the EOF were determined by two complementary procedures. The first one consists on treating these quantities as free parameters, to be determined by searching for the best fit to the experimental data in a CALPHAD

optimization. The second procedure involves estimations based upon various kinds of comparisons with related structures. The optimization procedure was applied by Walder and Ipser [34] to treat the end-members "Ni_3" and "Ni_2" in their three-sublattice model for ζ-Ni_2In (hP6), further requiring that the EOF per mole of atoms on Ni should be the same, as well as to the end-member "In" in their model for the δ-NiIn (B2) phase. Alternatively, the estimation procedure was applied by them to the end-members "Ni_2" and "Ni" of the two-sublattice model for δ-NiIn (B2), and by Liu et al. [35] to the end-member "Ni_4" of the three-sublattice model for Ni_3Sn_HT (cF16). According to Table 9, the smallest discrepancies between the CALPHAD values and the *ab initio* results are found for the optimized EOF of "Ni_3" in the model for ζ-Ni_2In (hP6) (+5.8 kJ/mol), for the estimated EOFs of "Ni_2" in the model for δ-NiIn (B2) (−0.38 kJ/mol) and of "Ni_4" in the model for Ni_3Sn (HT) (cF16) (−8.38 kJ/mol), whereas the largest deviation, *viz.*, about 100 kJ/mol corresponds to the estimated EOF for the non-stable B2 structure of Ni. It is interesting to note that for the latter, the CALPHAD value was taken by Waldner and Ipser [34] from the modeling of the B2 phase in the Ni–Al system reported by Ansara et al. [52].

4. Summary and conclusions

The general purpose of this work is to contribute to the knowledge of the equilibrium structural, cohesive and electronic properties of several stable, metastable and non-stable intermetallic phases (IPs) of the Ni–In and Ni–Sn systems. Using the projector augmented wave method and the exchange and correlation functions of Perdew and Wang in the generalized gradient approximation (GGA), as well as those by Ceperley and Alder in the local-density approximation (LDA), we determined the lattice-parameters (LPs), molar volume (V_o), bulk modulus (B_o) and its pressure derivative (B_o'), the electronic density of states (DOS) and the energy of formation (EOF) from the elements of several Ni–In and Ni–Sn IPs. Specifically, the Ni_3In, Ni_2In, $Ni_{13}In_9$, NiIn, Ni_2In_3 and Ni_3In_7 stable phases and the new compounds Ni_7In_3 and Ni_5In_3, occurring around the Ni_2In composition range were included. Moreover, the low-temperature stable phases Ni_3Sn, Ni_3Sn_2, Ni_3Sn_4 and the metastable $NiSn_4$ phase of the Ni–Sn system were treated. In addition, several non-stable ("hypothetical") compounds involved in the most recent CALPHAD modeling of the Ni–In and Ni–Sn phase diagrams were studied. The calculated values are compared with experimental data and theoretical results from the literature. The key findings of the work are summarized in the following.

The GGA (LDA) calculations overestimate (underestimate) V_o of most of the stable Ni–In and Ni–Sn compounds The theoretical B_o values for Ni–In and Ni–Sn compounds obtained with the GGA are smaller than those from the LDA. The V_o and B_o values for compounds vary smoothly with composition. The calculated V_o values for Ni–In and Ni–Sn deviate negatively from a linear interpolation between the elements. For B_o the LDA yields negative deviations from linearity and the GGA yields smaller deviations of both signs.

The calculated DOS of the Ni–In and Ni–Sn compounds show similar characteristics and indicate metallic behavior. The main contribution comes from the Ni-3d electrons. This band narrows slightly and shifts to lower energies for the compounds with increasing In/Sn content at their equilibrium structures. There is mixing of this Ni-3d band with the In/Sn-5p band with a minor contribution of In/Sn-5s states. At lower energies the free – electron type contribution of the In/Sn-5s electrons dominates. Above the Fermi level, there is an hybridization between Ni-3d and In/Sn-5p orbitals. Since Sn has a larger number of p electrons (4) than In (3) the hybridization effect is expected to be stronger for the Ni–Sn IPs.

A comprehensive *ab initio* account of the Ni–In system, involving stable, metastable and hypothetical, model-generated compounds have been presented for the first time. The phases Ni_3In, Ni_2In, $Ni_{13}In_9$, NiIn, Ni_2In_3 and Ni_3In_7 occurring at low-temperature in the phase diagram and the new compounds Ni_7In_3 and Ni_5In_3 are found to be thermodynamically stable with respect to the elements Ni and In. Both GGA and LDA calculations indicate that the hP8 structure of the Ni_3In compound is more stable than the cP4 by approximately 2 kJ/mol, if the internal coordinates are allowed to relax. If they are fixed at the experimentally reported positions the relative hP8/cP4 stability is reversed. The phases Ni_3Sn, Ni_3Sn_2, Ni_3Sn_4 occurring at low-temperature in the phase diagram, as well as the metastable $NiSn_4$ compound are found to be thermodynamically stable with respect to the elements Ni and Sn.

Systematic differences are found between the 0 K *ab initio* calculated EOFs and the experimental data at finite temperature for both binary systems. For Ni–In compounds, the differences between the calculated and the experimental EOF vary between 2.5 and 12.6 kJ/mol when the GGA is adopted, which decrease in magnitude with values of up to 8.3 kJ/mol with the LDA. For the Ni–Sn compounds, differences of 10.8 kJ/mol are found using the GGA, which decrease by about 5.4 kJ/mol when the LDA is adopted.

Calculations of the EOF were also performed for the end-member compounds (EMC) involved in the CALPHAD modeling of the δ-NiIn, ζ-Ni_2In and ζ'-$Ni_{13}In_9$ phases of the Ni–In system and the Ni_3Sn, Ni_3Sn_2, Ni_3Sn_4 phases of the Ni–Sn system. The *ab initio* 0 K values are used to compare with the results of the modeling work at 298.15 K and to characterize various key features of the CALPHAD predictions and estimations for non-stable compounds. For most of the EMC representing binary Ni–In and Ni–Sn compounds, the *ab initio* method leads to differences of ±15 kJ/mol with the CALPHAD values for EOF. In the case of the EMC representing non-stable structures of Ni and In, the typical difference might be as high as ±35 kJ/mol. However, for the B2 structure of Ni the difference amounts at 100 kJ/mol.

The new theoretical information is used to study the structure dependence upon the EOF, and the effect upon this quantity of different occupation schemes of the crystallographic sites consistent with the thermodynamic sublattices. The present discussion should be useful in attempts to complement the thermodynamic optimization techniques with *ab initio* values, and to gain insight on the effect of the approximations involved in the estimation procedures adopted in current CALPHAD modeling work.

Acknowledgements

This work was supported by Agencia Nacional de Promoción Científica y Tecnológica (BID 1728/OC-AR, PICT-2006 1947) and Universidad Nacional del Comahue (Project I157).

References

[1] W. Köster, T. Gödecke, D. Heine, Z. Metallkd. 63 (1972) 802–807.
[2] K.N. Tu, K. Zeng, Mater. Sci. Eng. R34 (2001) 1–58.
[3] K.N Subramanian, Lead-free Electronic Solders, A Special Issue of the Journal of Materials Science: Materials in Electronics, Springer, 2006.
[4] Ch-Yu Huang, S.-W. Chen, J. Electon. Mater. 31 (2002) 152–160.
[5] L. Kaufman, H. Bernstein, Computer Calculation of Phase Diagrams, Academic Press, New York, 1970.
[6] M. Hillert, J. Alloys Compd. 320 (2001) 161–176.
[7] M.F. Singleton, P. Nash, in: T. Massalski (Ed.), Binary Alloys Phase Diagrams, vol. 3, second ed., ASM, The Materials Information Society, 1990
[8] P. Villars, Pearsons, Handbook of Crystallographic Data for Intermetallic Phases, Desk Edition, ASM, Materials Park, OH 2, 1997, p. 2189.
[9] Ph. Durussel, G. Burri, P. Feschotte, J. Alloys Compd. 257 (1997) 253–258.
[10] L. Norén, R.L. Withers, Y. Tabira, J. Alloys Compd. 309 (2000) 179–187.
[11] L. Norén, A.-K. Larsson, R.L. Withers, H. Rundlöf, J. Alloys Compd. 424 (2006) 247–254.
[12] G.Y. Guo, Y.K. Wang, Li-Shing Hsu, J. Magn. Magn. Mater. 239 (2002) 91–93.
[13] G.Y. Guo, Y.-K. Wang, Li-Shing Hsu, Phys. Rev. B 66 (2002) 054440–054448.

[14] P. Blaha, K. Schwarz, J. Luitz, WIEN97, Vienna University of Technology, 1997.
[15] J.P. Purdew, S. Burke, M. Ernzerhof, Phys. Rev. Lett. 77 (1996) 3865–3868.
[16] Li. Shing Hsu, Y.-K. Wang, Y.-L. Tai, J.-F. Lee, J. Alloys Compd 413 (2006) 11–16.
[17] C. Deluque Toro, S. Ramos de Debiaggi, A.M. Monti, Physica B 407 (2012) 3236–3239.
[18] A.S. Mikhaylushkin, T. Sato, S. Carlson, S.I. Simak, U. Häussermann, Phys. Rev. B 77 (2008) 014102–014108.
[19] P.E. Blöchl, Phys. Rev. B 50 (1994) 17953–17979;
G. Kresse, J. Joubert, Phys. Rev. B 59 (1999) 1758–1775.
[20] J.P. Perdew, Y. Wang, Phys. Rev. B 45 (1992) 13244–13249.
[21] T.B. Massalski, H. Okamoto, P.R. Subramanian, L. Kacprak (Eds.), Binary Alloy Phase Diagrams, second ed., ASM, Materiasl Park, OH, 1990. p. 2863.
[22] H.R. Pak, T. Saburi, S. Nenno, Bull. Jpn. Inst. Met. 37 (1973) 1128–1134.
[23] A. Leineweber, M. Ellner, E.J. Mittermeijer, J. Solid State Chem. 159 (2001) 191–197.
[24] A. Leineweber, O. Oeckler, U. Zachwieja, J. Solid State Chem. 177 (2004) 936–945.
[25] A. Leineweber, J. Solid State Chem. 177 (2004) 1197–1212.
[26] A. Leineweber, E.J. Mittermeijer, M. Knapp, C. Baehtz, Philos. Mag. 87 (2007) 1821–1844.
[27] C. Schmetterer, H. Flandorfer, K.W. Richter, U. Saeed, M.M. Kauffman, P. Roussel, H. Ipser, Intermetallics 15 (2007) 862–884.
[28] S. Furuseth, H. Fjellvag, Acta Chem. Scand. 40A (1986) 695–700.
[29] W.J. Boettinger, M.D. Vaudin, M.E. Williams, L.A. Bendersky, W.R. Wagner, J. Electron. Mater. 32 (2003) 511–515.
[30] T. Watanabe, K. Arai, T. Hirose, M. Chikazawa, J. Jpn. Inst. Met. 63 (1999) 496–501.
[31] G. Ghosh, Metall. Mater. Trans. A 40 (2009) 4–23.
[32] S. Ramos de Debiaggi, C. Deluque Toro, G. Cabeza, A. Fernández Guillermet, J. Alloys Compd. 542 (2012) 280–292.
[33] A. Fernández Guillermet, Assessment of phase stability and thermochemistry of high-melting alloys and compounds: a systematic approach based on Gibbs energy modelling, in: K.E. Spear (Ed.), Proc. Nineth International Conference on High Temperature Materials Chemistry, The Electrochemical Society Proceedings, vol. 97, Pennington, New York, 1997, pp. 135–144.
[34] P. Waldner, H. Ipser, Z. Metallkd. 93 (2002) 825–832.
[35] H.S. Liu, J. Wang, Z.P. Jin, CALPHAD 28 (2004) 363–370.
[36] G. Kresse, J. Furthmüller, Comput. Mater. Sci. 6 (1996) 15–50.
[37] D.M. Ceperley, B.J. Alder, Phys. Rev. Lett. 45 (1980) 565–569.
[38] R.O. Jones, O. Gunnarsson, Rev. Mod. Phys. 61 (1989) 689–746.
[39] J.P. Perdew, J.A. Chevary, S.H. Vosko, K.A. Jackson, M.R. Pederson, D.J. Singh, C. Fiolhais, Phys. Rev. B 46 (1992) 6671–6687.
[40] C. Fiolhais, F. Nogueira, M. Marques (Eds.), A Primer in DENSITY Functional theory, Springer, 2003.
[41] H.J. Monkhorst, J.D. Pack, Phys. Rev. B 13 (1976) 5188–5192.
[42] M. Methfessel, A.T. Paxton, Phys. Rev. B 40 (1986) 3616–3621.
[43] P. Vinet, J.H. Rose, J. Ferrante, J.R. Smith, J. Phys.: Condens. Matter 1 (1989) 1941–1963.
[44] S. Ramos de Debiaggi, G.F. Cabeza, C. Deluque Toro, A.M. Monti, S. Sommadossi, A. Fernández Guillermet, J. Alloys Compd. 509 (2011) 3238–3245.
[45] G. Ghosh, M. Asta, J. Mater. Res. 20 (2005) 3102–3117.
[46] M. Fuchs, J.L.F. Da Silva, C. Stampfl, J. Neugebauer, M. Scheffler, Phys. Rev. B. 65 (2002) 24512–24513.
[47] J.L.F. Da Silva, C. Stampfl, M. Scheffler, Surf. Sci. 600 (2006) 703–715.
[48] G. Ghosh, M. Asta, Acta Mater. 53 (2005) 3225–3252.
[49] J.F. Janak, Phys. Rev. B 16 (1977) 255–262.
[50] M.S.S. Brooks, O. Eriksson, B. Johansson, J.J.M. Franse, P.H. Frings, J. Phys. F: Met. Phys. 18 (1988) L33–L39.
[51] Y. Wang, S. Curtarolo, C. Jiang, R. Arroyave, T. Wang, G. Ceder, L.-Q. Chen, Z.-K. Liu, CALPHAD 78 (2004) 79–90.
[52] I. Ansara, N. Dupin, H. Lukas, B. Sundman, J. Alloys Compd. 247 (1997) 20–30.
[53] R. Kolhaas, P. Dünner, N. Schmitz-Pranghe, Z. Angew. Phys. 23 (1967) 245–247.
[54] G. Alers, J.R. Neighbours, J. Phys. Chem. Solids 13 (1960) 40–55.
[55] D.J. Steinberg, J. Phys. Chem. Solids 43 (1982) 1173–1175.
[56] D.H. Martin, Magnetism in Solids, The MIT Press, Cambridge, MA, 1967. p. 10.
[57] J. Bandopadhay, K.P. Gupta, Cryogenics 17 (1977) 345–347.
[58] I. Nakai, F. Ono, O. Yamada, J. Phys. Soc. Jpn. 52 (1983) 1791–1798.
[59] K. Takemura, Phys. Rev. B 44 (1991) 545–549.
[60] J.A. Rayne, B.S. Chandrasekhar, Phys. Rev. 120 (1960) 1658–1663.
[61] A.L. Lyubimtsev, A.I. Baranov, A. Fischer, L. Kloo, B.A. Popovkin, J. Alloys Compd. 340 (2002) 167–172.
[62] J. Schmid, M. Bienzle, F. Sommer, B. Predel, Z. Metallkd. 86 (1995) 877.
[63] G. Ghosh, Metall. Mater. Trans. A 30A (1999) 1481–1494.
[64] P. Nash, H. Choo, R.B. Schwarz, J. Mater. Sci. 33 (1998) 4929–4936.
[65] G.P. Vassilev, K.I. Lilova, J.C. Gachon, J. Alloy. Compd. 447 (2006) 106–108.
[66] R. Hultgren, P. Desai, P. Hawkins, M. Gleiser, K.K. Kelley, Selected Values of the Thermodynamic Properties of Binary Alloys, ASM, Metals Park, OH, 1973, pp. 1237–1239.
[67] B. Predel, H. Ruge, Thermochim. Acta 3 (1972) 411–419.
[68] W.B. Pearson, L.T. Thompson, Can. J. Phys. 35 (1957) 349–357.
[69] H. Flandorfer, U. Saeed, C. Luef, A. Sabbar, H. Ipser, Thermochim. Acta 459 (2007) 34–39.